

## 14. EOLIAN AND SILICA DEPOSITION IN THE CENTRAL NORTH PACIFIC: RESULTS FROM SITES 885/886<sup>1</sup>

Hilde Snoeckx,<sup>2</sup> David K. Rea,<sup>2</sup> Charles E. Jones,<sup>2</sup> and B. Lynn Ingram<sup>3</sup>

### ABSTRACT

Sediments recovered at Ocean Drilling Program Sites 885/886 (central North Pacific Ocean at 44°41'N, 168°14'W and 44°41'N, 168°16'W, respectively) record eolian deposition during the Cenozoic and late Mesozoic. We constructed a record of eolian MAR, which is a proxy for aridity/humidity of the climate in the continental source area. Eolian fluxes are low during the Late Cretaceous through Eocene, reflecting humid conditions in the source area. During the Oligocene, more arid climates prevailed at the source area, as indicated by increased eolian accumulation. The "Diatom Dump", an interval of enhanced silica deposition mainly apparent in the northwest Pacific, is reflected in the record at Sites 885/886 by two- to fivefold higher opal fluxes compared with younger and older sediments. Increased eolian deposition starting at 3.5 Ma and culminating at 2–2.6 Ma are coincident with the onset of Northern Hemisphere glaciation. Sites 885/886 lie 10° north of sites examined previously for the history of eolian deposition in the central North Pacific and therefore allow enhanced understanding of the latitudinal variation of the wind system.

### INTRODUCTION

One of the objectives of Ocean Drilling Program (ODP) Leg 145 was to investigate the history of Cenozoic and Late Cretaceous atmospheric circulation provided by eolian sediments in the North Pacific. For that purpose, Sites 885 and 886 were drilled 1 km apart at 44°41'N, 168°16'W and 168°14'W, respectively, at about 5700 m water depth (Fig. 1). The sites are underneath the northern edge of the low-productivity zone of the central gyre. More importantly, they are located downwind from Asia, presumed to be the main source area for dust throughout the Cenozoic (Rea et al., 1985; Kyte et al., 1993; Nakai et al., 1993). Also, their location is sufficiently far removed from the continent to preclude influence of riverine input and ice-rafted debris.

The flux of windblown particles transported to the ocean is mainly dependent on the availability of deflatable material and therefore a proxy of humid-arid continental climate conditions (Prospero, 1981; Rea et al., 1985; Pye, 1989).

Earlier studies in the north Pacific Ocean covering the Cenozoic and late Mesozoic were performed on data from Deep Sea Drilling Project (DSDP) Site 576 (32°N, 164°E) by Janecek (1985), piston Core LL44-GPC3 (30°N, 158°W) by Janecek and Rea (1983), and DSDP Site 464 (40°N, 174°E) by Rea and Harsch (1981). This last site provided only a discontinuous record of eolian influx because of the low recovery and long hiatuses (Rea and Harsch, 1985).

Whole Cenozoic records of eolian deposition were obtained from DSDP Site 576 and piston Core LL44-GPC3. During the Late Cretaceous and the Paleocene, eolian mass accumulation rates (MARs) at these sites were low, corresponding to warm and wet climates. During the middle to late Eocene the records of DSDP Site 576 and Core LL44-GPC3 show a decrease in eolian MARs that may be the result of a more humid climate in the eolian source region and/or the passage of those sites from one wind belt to another (Leinen and Heath, 1981; Janecek and Rea, 1983; Rea, 1994). Accumulation rates at those sites were found to be low in the Oligocene which contradicts the notion of drier climates in the Oligocene than in the Paleocene and Eocene suggested by other climatic data (Janecek, 1985).

The record obtained at Sites 885/886, which are the northernmost sites studied thus far for their eolian signal, provides an opportunity to establish longitudinal transects and to make comparisons with data from farther to the south, such as at DSDP Site 576 and in Core LL44-GPC3.

### METHODS

#### Sample Strategy

The eolian record for Sites 885/886 was determined from samples from Holes 885A, 886B, and 886C. Samples were taken over the entire length of the sediment column of Holes 885A and 886B and the bottom of Hole 886C (Cores 7H and 8H). The three holes, as well as Hole 886A, were placed on a common depth scale based on the magnetic susceptibility record, using the chemostratigraphy and dust records as independent controls (Dickens et al., this volume). The records for Holes 885A and 886B largely overlap, and drilling in Hole 886C extended the record to basement and provided a comfortable overlap of 8 m with Hole 886B. Samples from Holes 886B and 886C were analyzed at a spacing of four samples per 1.5-m section. Hole 885A was analyzed with a sample frequency of two samples per section to provide a control; because of stratigraphic ambiguity in the top 10 m of Hole 886B (Dickens et al., this volume), the sample frequency was increased to four samples per 1.5-m section in the top 12.6 mbsf.

#### Extraction of the Eolian Component

The eolian component of the sediments was isolated using a modified version of the extraction procedure detailed by Rea and Janecek (1981). The procedure calls for the removal of calcium carbonate by acetic acid. Because Sites 885/886 are beneath the calcite compensation depth, we did not expect to find CaCO<sub>3</sub> in the sediment. Amorphous Fe and Mn oxides and hydroxides, as well as zeolites were removed with a buffered sodium citrate and sodium dithionite solution. The increased accumulation of hydrothermal material at the bottom of Hole 886C (Dickens and Owen, this volume) required repeated applications of this procedure. Parallel analyses of low oxy-hydroxide samples from the same site do not indicate additional clay loss after repeating this step. Opaline silica in the Rea and Janecek (1981) method is removed by sodium carbonate. However, this digestant is inadequate in removing all of the biogenous silica for sediments at these sites. Therefore, opal was dissolved by the harsher sodium hydroxide. Unlike Hovan's (in press) experience with equa-

<sup>1</sup> Rea, D.K., Basov, I.A., Scholl, D.W., and Allan, J.F. (Eds.), 1995. *Proc. ODP, Sci. Results*, 145: College Station, TX (Ocean Drilling Program).

<sup>2</sup> Department of Geological Sciences, University of Michigan, 1006 C.C. Little Building, Ann Arbor, MI 48109-1063, U.S.A.

<sup>3</sup> Department of Geology and Geophysics, University of California, Berkeley, CA 94720, U.S.A.

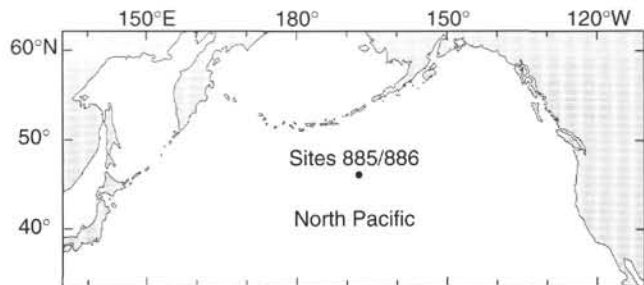


Figure 1. Map of the North Pacific Ocean showing Sites 885/886.

torial Pacific samples, we did not observe a quantifiable leaching of the crystalline silicate component. Different clay mineralogy and a relatively greater amount of dissolution-prone neoformal mineral in the low-dust equatorial sediments may explain the difference. The extraction procedure does not remove volcanic ash. We took care not to sample ash layers but samples younger than 2.6 Ma may contain minute amounts of disseminated ash. Results of the extraction method are tabulated in Table 1.

### Siliceous Component

To the extent that sediments at Sites 885/886 are a two-component system of biogenous silica and eolian dust (i.e., above ~54 meters composite depth [mcd]), the amount of opal can be estimated by the difference:

$$\text{wt\% opal} = 100 - \text{wt\% dust.}$$

Calculated amounts of opal are presented in Table 1.

### Mass Accumulation Rate Calculations

The mass accumulation rate (MAR) is the product of the linear sedimentation rate (LSR) and the dry bulk density of the sample. The flux of the windblown component and of opal is the product of the percentage by weight of the respective component and the total sediment MAR. For example,

$$\text{eolian MAR [g/(cm}^2 \cdot \text{k.y.)]} = \% \text{ extracted} \times \text{LSR (cm/k.y.)} \\ \times \text{DBD (g/cm}^3\text{)}.$$

The MAR of the eolian and biogenous component was calculated based on assumptions related to depth, age, and dry bulk density of the sample as outlined below. All data are tabulated in Table 1. The accuracy of the MARs strongly depends on the accuracy of the stratigraphy. In view of the assumptions described here, care should be taken in interpreting the eolian flux. Changes in eolian MAR of less than 10%–20% above 52 mcd (or 8.5 Ma) and of 50%–100% in the older sediments are geologically not significant.

### Dry Bulk Density

Dry bulk density was calculated from onboard physical properties measurements (Rea, Basov, Janecek, Palmer-Julson, et al., 1993). One 10-cm<sup>3</sup> sample was taken per section. The index properties (wet-bulk density, grain density, water content, porosity, and dry-bulk density) were determined from measurements of wet and dry weights and dry volume (Rea, Basov, Janecek, Palmer-Julson, et al., 1993). We calculated dry bulk densities by interpolation between these known values.

### Composite Depth Scale

The eolian record for Sites 885/886 is a composite based on the record of three holes. Therefore, it was necessary to place all samples on a common depth scale, termed meters composite depth. To this end

a composite depth scale was established (Dickens et al., this volume). Because of stratigraphic ambiguity in the top of Hole 886B, no composite depths are calculated for the interval between 0 and 10.25 mbsf. The composite depth scale for Sites 885/886 stretches the sediment column for each hole, by approximately 8% in the case of Hole 886B to 10% for the top 10 m and 40% below 10 m in the case of Hole 885A. No stretching was done in Hole 886C for the depth interval studied. The use of a composite depth scale, therefore, may increase the LSR and would therefore lead to exaggerated MARs. The eolian record for Sites 885/886 has been assembled from segments of the three holes: between 0 and 10.25 mcd in samples from Hole 885A, from 10.25 to 60 mcd in samples from Hole 886B, and from 60 mcd to basement in samples from Hole 886C. This composite record ensures that the error in the LSR caused by stretching or compression is minimal and negligible compared with the uncertainties in the time scale.

### Age Model

The time scale adopted by the Leg 145 scientific party was constructed by Cande and Kent (1992). The age model (Fig. 2) for the upper 52 mcd is based on the magnetic reversal stratigraphy (Rea, Basov, Janecek, Palmer-Julson, et al., 1993) and radiolarian stratigraphy (Morley and Nigrini, this volume). In general, radiolarian events support the magnetic reversal stratigraphy (Fig. 2). The age model based on these two stratigraphies is reliable to 8.5 Ma.

Below 53 mcd, the sediment column is devoid of identifiable microfossils except for occasional fish remains. As a consequence, the sedimentation rate drops to a level too low for reliable magnetostratigraphy. The age of the oldest sediment is constrained by the age of the basement, which is  $80 \pm 1$  Ma (Keller and Duncan, this volume). The Cretaceous/Tertiary (K/T) stratum was placed in Core 145-886C-8H between 130 and 145 cm, which corresponds to 63.25–63.4 mcd (Kye and Zhou, this volume). A time resolution of three strata, which are 56.5 and 15 m.y. apart, respectively, inhibits the study of any climatic or geologic signals for this period. To improve the time resolution, the Sr-isotope stratigraphy determined from ichthyoliths was used as an alternative dating method (Ingram, this volume). All stratigraphic data considered for the age model are presented in Table 2.

### Sr Isotopes and Fish Teeth: A Tartar Removal Experiment

The Sr-isotope seawater curve recorded by ichthyoliths promises to provide a useful relative dating method for red-clay sites, where dating traditionally has been difficult. Previous work on fish teeth showed that, although they can retain <sup>87</sup>Sr/<sup>86</sup>Sr signatures that are close to the primary marine signal (Staudigel et al., 1985), several samples did in fact yield <sup>87</sup>Sr/<sup>86</sup>Sr ratios that were significantly different from what would be expected from their stratigraphic ages. We picked fish teeth from eight samples from Hole 886C for Sr isotopic analysis. The main goal of this pilot study was to determine whether the main source of error in ichthyolith analyses resides in the Fe-Mn oxide coatings commonly found on fish teeth, in the incomplete cleaning of samples, or in the preservation of the fish teeth themselves.

Fish teeth handpicked from sieved sediment samples were washed with distilled water. To remove any transition-metal oxide coatings, all samples were subjected to the reductive dissolution technique described by Mehra and Jackson (1960) and Rea and Janecek (1981). Two mL of 0.3 M sodium citrate and 0.25 mL of 1.0 M sodium bicarbonate were added to each beaker and heated to near-boiling. Then, approximately 0.05 g of sodium dithionite was added and the capped Teflon perfluoroalkoxy (PFA) beakers were placed in an ultrasonic bath for 30 min. Because of the very small sample size, just one application of this treatment appeared to remove all visible Fe-oxide coatings. Before this treatment, samples from greater depths (Table 3) appeared under a binocular microscope to be heavily coated with Fe oxides and to have their hollow cores also filled with oxides. After the

reductive dissolution, all fish teeth except for two exceptionally large specimens (~1 mm in length) became translucent such that it was difficult to see them against their semitranslucent Teflon background. No sign of oxide staining or residual clay minerals was present on either the outside or inside of any tooth. The two large teeth, one of which had been bored and appeared to be (bio?)corroded (Table 3), were too large to be translucent; nevertheless they showed no sign of oxide staining on the outside surfaces. Because of the translucence of the teeth, it was necessary to use a pipette under the binocular microscope to avoid losing the fish teeth while decanting the reductive solution. The samples were then rinsed twice using 7 mL of ultrapure water and placed in the ultrasonic bath for 30 minutes. This rinsing was intended to remove as much as possible of the Sr associated with both the Fe oxide coatings and with the reagents used for the reductive dissolution. The fish teeth were then transferred to fresh acid-cleaned Teflon beakers, dissolved in 0.2 mL 3 M ultrapure nitric acid, and loaded onto SrSpec columns with a resin bed volume of 0.07 mL. Major elements were eluted with 1 mL 3 M nitric acid, and the purified Sr was collected in 1 mL of water. The Sr was loaded onto Re single filaments with a TaCl<sub>3</sub> solution and 5% phosphoric acid and analyzed on a VG Sector multicollector thermal ionization mass spectrometer in multidynamic analysis mode. Samples were normalized to <sup>86</sup>Sr/<sup>88</sup>Sr = 0.1194; total procedural blanks were < 40 pg. The sample details and Sr isotopic results are presented in Table 3.

It seems possible that the somewhat scattered results of Staudigel et al. (1985) are caused by the variable inclusion of contaminant Sr associated with the Fe-Mn oxide coatings. Our results support the likelihood that fish teeth retain a primary marine <sup>87</sup>Sr/<sup>86</sup>Sr signature. However, despite this important result, the data presented in Table 3 should still be viewed with some caution. For example, the Ir anomaly was located about 30 cm above interval 145-886C-8H-2, 10–15 cm (Kyte, this volume), thus dating this sample as older than the K/T boundary. However, the <sup>87</sup>Sr/<sup>86</sup>Sr ratio of the fish teeth from this level would indicate an age of approximately 33 Ma, based on a comparison with the seawater Sr-isotope record. It would require a lowering of the measured ratio by roughly 0.000080 to be consistent with a latest Cretaceous age. In addition, a sample taken from interval 145-886C-7H-6, 10–15 cm, and analyzed by Ingram (this volume) has yielded a <sup>87</sup>Sr/<sup>86</sup>Sr ratio 0.000080 higher than the ratio measured in this work. Fish teeth from this level do not have visible coatings; our cleaning procedure, therefore, is less likely to have removed any contaminating Sr associated with any oxide phases. The fact that intervals 145-886C-8H-2, 10–15 cm, and -7H-6, 10–15 cm yielded ratios that appear to be too high may indicate that there may be some contamination associated with a residual amount of the reductive dissolution reagents. Because the fish teeth were transferred to fresh beakers, this potential contamination, which was not removed by the double water rinses, may be either associated with material on the fish tooth surfaces or with material left in the tiny conical cavities of the fish teeth. Any future work on fish teeth should include more rigorous rinsing, perhaps with a pure ammonium chloride solution or acetic acid (cf. Bertram et al., 1992).

### Backtrack and Paleolatitude (Paleoposition)

Because wind patterns may change in time and space, it is fundamental to the interpretation of the eolian signal to know the paleoposition of Sites 885/886. The backtrack path (Fig. 3) was drawn after the model proposed by van Andel et al. (1975) and modified by Prince (1978). The same model was used by Leinen and Heath (1981) for piston Core LL44-GPC-3.

## RESULTS

### Eolian Abundance

The eolian dust record shows very good agreement among the different holes (Fig. 4) and presents an independent test for the composite depth scale (Dickens et al., this volume).

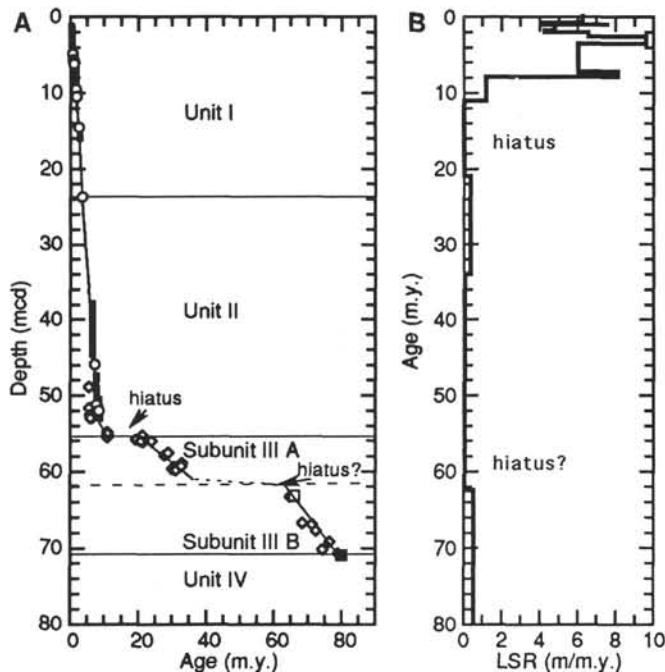


Figure 2. A. Age-depth model for Sites 885/886 based on magnetic reversal stratigraphy (Rea, Basov, et al., 1993), radiolarian stratigraphy (Morley and Nigrini, this volume), Sr-isotope stratigraphy (Ingram, this volume; this paper), Ir anomaly (Kyte and Zhou, this volume), and Ar/Ar dating (Keller and Duncan, this volume). Open circles represent paleomagnetic reversals; diamonds represent ichthyoliths (fish teeth), the open square represents the Ir anomaly that indicates the Cretaceous/Tertiary boundary; and the closed square represents basement. Solid thick lines represent the depth range of radiolarian events. Also shown are lithologic units from Rea, Basov, Janecek, Palmer-Julson, et al. (1993), as modified by Dickens et al. (this volume). B. Linear sedimentation rates calculated from the age-depth model.

Three major lithologic units are recognized in Sites 885/886 (Fig. 5) (Rea, Basov, Janecek, Palmer-Julson, et al., 1993). The boundaries of the units described here have been adjusted to the composite depth scale according to Dickens et al. (this volume). Unit I, between 0 and 23.75 mcd and 53 mcd, consists mainly of clay with diatoms; Unit II, between 23.75 and 53 mcd, of diatom ooze and clayey diatom ooze; and Unit III of clay and hematitic clay (Rea, Basov, Janecek, Palmer-Julson, et al., 1993). A reinterpretation of Unit III suggests subdivision at 62 mcd into Subunit IIIA, which is predominantly clay, and Subunit IIIB, which consists mainly of distal hydrothermal Fe-Mn precipitates (Dickens et al., this volume). The abundance of extracted eolian material in Unit I is 40%–55% (Fig. 5) in the top 18 mcd and decreases gradually to 20% toward the bottom of this unit. A sharp plunge in the percentage of eolian material occurs at approximately 16 mcd (Fig. 5). This anomalous interval is also present in the geochemical record (Dickens et al., this volume). Unit II is marked by two lithologies: diatom ooze above 48 mcd and clayey diatom ooze below. Within the diatom ooze interval, there are two levels in eolian abundances: above 35 mcd eolian abundance is low (10% or less) whereas below 35 mcd, abundance varies from 10% to 20% (Fig. 5). In the clayey diatom ooze (between 48 and 55 mcd) the eolian component varies from 20% to 45% (Fig. 5). Subunit IIIA contains 25% to 40% dust, whereas the amount of extracted material decreases to nearly nil toward the basement in Subunit IIIB (Fig. 5).

### Opal Abundance

As expected, the record of opal is the mirror image of the eolian record (Figs. 5 and 6). The amount of biogenic silica is roughly equal to the windblown sediment in the top 18 m of the sediment column,

Table 1. Data from Sites 885/886.

Core, section interval (cm)	Depth (mbsf)	Depth (mcd)	Age (m.y.)	LSR (m/m.y.)	DBD (g/cm <sup>3</sup> )	Eolian (wt%)	Eolian MAR (mg/[cm <sup>2</sup> ·k.y.])	Opal (wt%)	Opal MAR (mg/[cm <sup>2</sup> ·k.y.])
145-885A-									
1H-1, 30-35	0.30	0.35	0.06	6.3	0.47	45.6	134	54.4	160
1H-1, 55-60	0.55	0.71	0.11	6.3	0.47	47.9	141	52.1	153
1H-1, 105-110	1.05	1.40	0.22	6.3	0.46	51.0	148	49.0	142
1H-1, 130-135	1.30	1.71	0.27	6.3	0.46	52.4	150	47.6	137
1H-2, 30-35	1.80	2.40	0.38	6.3	0.45	48.1	135	51.9	145
1H-2, 55-60	2.05	2.74	0.44	6.3	0.44	52.3	145	47.7	132
1H-2, 105-110	2.55	3.47	0.55	6.3	0.45	48.9	139	51.1	145
1H-3, 30-35	3.30	4.47	0.71	6.3	0.48	36.9	111	63.1	189
1H-3, 55-60	3.55	4.60	0.74	6.3	0.49	38.9	119	61.2	187
1H-3, 105-110	4.05	5.00	0.81	4.1	0.50	50.5	103	49.5	101
1H-3, 130-135	4.30	5.25	0.87	4.1	0.50	52.5	107	47.5	97
2H-1, 30-35	4.90	5.65	0.97	4.1	0.51	54.0	111	46.1	95
2H-1, 55-60	5.15	5.91	1.01	7.5	0.51	50.8	195	49.2	189
2H-1, 105-110	5.65	6.46	1.10	4.8	0.50	49.4	118	50.6	121
2H-1, 130-135	5.90	6.73	1.16	4.8	0.49	45.6	107	54.4	128
2H-2, 30-35	6.40	7.27	1.28	4.8	0.47	47.0	107	53.0	121
2H-2, 53-58	6.63	7.52	1.33	4.8	0.47	40.4	91	59.6	134
2H-2, 105-110	7.15	8.01	1.43	4.8	0.47	45.5	104	54.5	124
2H-2, 130-135	7.40	8.23	1.48	4.8	0.49	45.0	105	55.0	128
2H-3, 30-35	7.90	8.67	1.57	4.8	0.51	40.6	99	59.4	145
2H-3, 55-60	8.15	8.90	1.62	4.8	0.52	49.8	125	50.2	125
2H-3, 105-110	8.65	9.42	1.73	4.8	0.51	50.1	121	49.9	121
2H-3, 130-135	8.90	9.77	1.81	4.3	0.49	40.4	84	59.6	124
2H-4, 30-35	9.40	10.43	1.96	4.3	0.45	48.0	92	52.0	99
2H-4, 105-110	10.15	11.76	2.17	6.6	0.42	40.1	110	59.9	165
2H-4, 130-135	10.40	12.32	2.26	6.6	0.42	47.0	131	53.0	148
2H-5, 30-35	10.90	1.35	2.41	6.6	0.44	41.3	119	58.7	169
2H-5, 55-60	11.15	13.85	2.49	6.6	0.44	31.4	92	68.6	201
2H-5, 105-110	11.65	14.73	2.62	6.6	0.43	43.2	123	56.8	162
2H-5, 130-135	11.90	15.07	2.67	6.6	0.42	38.5	106	61.5	170
2H-6, 30-35	12.40	15.76	2.72	9.6	0.39	14.7	56	85.3	323
2H-6, 55-60	12.65	16.10	2.76	9.6	0.38	22.9	84	77.1	282
2H-6, 105-110	13.15	16.79	2.83	9.6	0.37	26.2	93	73.8	261
2H-6, 130-135	13.40	17.11	2.86	9.6	0.37	24.2	85	75.8	268
3H-1, 30-35	14.40	20.00	3.16	9.6	0.36	22.4	78	77.6	270
3H-1, 105-110	15.15	21.12	3.28	9.6	0.37	19.5	70	80.5	290
3H-2, 30-35	15.90	22.60	3.43	9.6	0.41	18.9	75	81.1	319
3H-2, 105-110	16.65	23.35	3.51	9.6	0.41	13.2	52	86.8	342
3H-3, 30-35	17.40	24.10	3.61	6.0	0.36	10.0	22	90.1	195
3H-3, 105-110	18.15	24.85	3.74	6.0	0.33	10.0	20	90.0	178
3H-4, 30-35	18.90	25.60	3.86	6.0	0.32	8.6	17	91.4	178
3H-4, 105-110	19.65	26.35	3.98	6.0	0.31	9.4	18	90.6	171
3H-5, 30-35	20.40	27.10	4.11	6.0	0.30	8.0	14	92.0	166
3H-5, 105-110	21.15	17.85	4.23	6.0	0.29	5.2	9	94.8	167
3H-6, 30-35	21.90	28.60	4.36	6.0	0.30	5.3	9	94.7	169
3H-6, 105-110	22.65	29.35	4.48	6.0	0.32	3.5	7	96.5	186
3H-1, 30-35	23.40	30.10	4.61	6.0	0.37	3.3	7	96.7	216
4H-1, 30-35	23.90	29.45	4.50	6.0	0.39	4.2	10	95.8	224
4H-1, 105-110	24.65	30.20	4.62	6.0	0.30	4.2	7	95.8	170
4H-2, 30-35	25.40	30.95	4.75	6.0	0.31	4.8	9	95.2	178
4H-2, 105-110	26.15	31.70	4.87	6.0	0.34	5.7	12	94.3	191
4H-3, 30-35	26.90	32.40	4.99	6.0	0.38	4.6	11	95.4	216
4H-3, 105-110	27.65	33.06	5.10	6.0	0.40	18.0	43	82.0	196
4H-4, 30-35	28.40	33.71	5.21	6.0	0.39	12.6	29	87.4	203
4H-4, 105-110	29.15	34.36	5.32	6.0	0.39	8.7	20	91.3	216
4H-5, 28-33	29.88	35.00	5.42	6.0	0.42	18.5	47	81.5	207
4H-5, 105-110	30.65	35.82	5.56	6.0	0.43	16.2	42	83.8	216
4H-6, 30-35	31.60	36.87	5.73	6.0	0.39	12.0	28	88.0	206
4H-6, 105-110	32.15	37.48	5.83	6.0	0.42	9.7	25	90.3	229
4H-1, 30-35	32.90	38.17	5.95	6.0	0.52	17.2	54	82.8	260
5H-1, 30-35	33.40	39.20	6.12	6.0	0.56	20.5	70	79.5	270
5H-1, 105-110	34.15	39.95	6.24	6.0	0.43	23.2	60	76.8	199
5H-2, 30-35	34.90	40.74	6.37	6.0	0.39	12.1	28	87.9	205
5H-2, 105-110	35.65	41.69	6.53	6.0	0.37	17.1	38	82.9	183
5H-3, 30-35	36.40	42.72	6.70	6.0	0.38	14.1	32	85.9	197
5H-3, 105-110	37.15	43.66	6.86	6.0	0.38	10.1	23	89.9	206
5H-4, 30-35	37.90	44.55	7.01	6.0	0.35	9.7	21	90.3	193
5H-4, 105-110	38.65	45.44	7.16	6.0	0.37	11.2	25	88.8	198
5H-5, 30-35	39.40	46.34	7.29	8.1	0.45	14.4	52	85.6	311
5H-5, 105-110	40.15	47.23	7.40	8.1	0.49	25.1	99	74.9	296
5H-6, 30-35	40.90	48.19	7.52	8.1	0.48	35.0	136	65.0	252
5H-6, 105-110	41.65	49.21	7.64	8.1	0.46	30.9	116	69.1	258
5H-1, 30-35	42.40	50.10	7.75	8.1	0.43	28.1	99	71.9	254
6H-1, 30-35	42.90	50.60	7.81	8.1	0.41	27.1	90	72.9	242
6H-1, 105-110	43.65	51.44	8.05	1.2	0.39	34.6	16	65.4	30
6H-2, 30-35	44.40	52.38	8.84	1.2	0.42	45.7	23	54.3	28
6H-2, 105-110	45.15	53.15	9.47	1.2	0.44	50.8	27	49.2	27
6H-3, 30-35	45.90	53.82	10.02	1.2	0.45	44.5	24		
6H-3, 105-110	46.65	54.50	10.58	1.2	0.49	46.7	28		
6H-4, 30-35	47.40	55.17	11.13	1.2	0.57	42.4	29		
6H-4, 105-110	48.15	55.66	21.36	0.4	0.58	46.0	10		
6H-5, 30-35	48.90	59.04	30.40	0.4	0.49	37.6	7		
6H-5, 105-110	49.65	62.40	64.15	0.5	0.44	30.6	7		
6H-6, 30-35	50.40	63.15	65.54	0.5	0.45	22.5	5		
6H-6, 105-110	51.15	69.79	77.84	0.5	0.45	6.1	1		
6H-1, 30-35	51.78	70.38	78.94	0.5	0.42	4.9	1		

Table 1 (continued).

Core, section interval (cm)	Depth (mbsf)	Depth (mcd)	Age (m.y.)	LSR (m/m.y.)	DBD (g/cm <sup>3</sup> )	Eolian (wt%)	Eolian MAR (mg/[cm <sup>2</sup> ·k.y.])	Opal (wt%)	Opal MAR (mg/[cm <sup>2</sup> ·k.y.])
145-886B-									
1H-1, 30-35	0.30				0.48	45.8		54.2	
1H-1, 55-60	0.55				0.48	46.4		53.6	
1H-2, 30-35	1.50				0.51	43.5		56.5	
2H-1, 30-35	2.10				0.53	45.7		54.3	
2H-1, 55-60	2.35				0.54	51.5		48.5	
2H-1, 105-110	2.85				0.52	50.7		49.3	
2H-1, 130-135	3.10				0.50	49.9		50.1	
2H-2, 30-35	3.60				0.47	50.6		49.4	
2H-2, 55-60	3.85				0.45	46.0		54.0	
2H-2, 105-110	4.35				0.45	43.4		56.6	
2H-3, 30-35	5.10				0.47	46.7		53.3	
2H-3, 55-60	5.35				0.48	45.7		54.3	
2H-3, 105-110	5.85				0.49	44.3		55.7	
2H-3, 130-135	6.10				0.49	40.5		59.5	
2H-4, 30-35	6.60				0.50	45.0		55.0	
2H-4, 55-60	6.85				0.50	44.9		55.1	
2H-4, 105-110	7.35				0.51	53.4		46.6	
2H-4, 130-135	7.60				0.52	48.2		51.8	
2H-5, 30-35	8.10				0.52	47.8		52.2	
2H-5, 55-60	8.35				0.53	48.6		51.4	
2H-5, 105-110	8.85				0.54	50.1		49.9	
2H-5, 130-135	9.10				0.55	48.8		51.2	
2H-6, 30-35	9.60				0.56	47.2		52.8	
2H-6, 55-60	9.85				0.57	48.0		52.0	
2H-6, 105-110	10.35				0.56	52.4		47.6	
2H-7, 30-35	11.10				0.53	51.1		48.9	
2H-7, 55-60	11.35				0.52	45.9		54.1	
3H-1, 30-35	11.60				0.52	46.7		53.3	
3H-1, 55-60	11.85				0.51	44.3		55.7	
3H-1, 105-110	12.35				0.49	41.8		58.2	
3H-1, 130-135	12.60				0.48	36.0		64.0	
3H-2, 30-35	13.10	10.40	1.96	4.3	0.45	41.9	81	58.1	112
3H-2, 55-60	13.35	10.65	2.00	6.6	0.43	39.2	112	60.8	174
3H-2, 105-110	13.85	11.27	2.10	6.6	0.45	42.6	126	57.4	169
3H-2, 130-135	14.10	11.63	2.15	6.6	0.46	43.5	132	56.5	171
3H-3, 30-35	14.60	12.33	2.26	6.6	0.48	44.0	140	56.0	178
3H-3, 55-60	14.85	12.69	2.31	6.6	0.49	37.2	121	62.8	204
3H-3, 105-110	15.35	13.39	2.42	6.6	0.49	40.8	130	59.2	189
3H-3, 130-135	15.60	13.74	2.47	6.6	0.48	36.5	114	63.5	199
3H-4, 30-35	16.10	14.45	2.58	6.6	0.46	40.5	121	59.5	179
3H-4, 55-60	16.35	14.70	2.61	9.6	0.45	40.5	174	59.5	255
3H-4, 105-110	16.85	15.20	2.66	9.6	0.43	33.1	137	66.9	277
3H-4, 130-135	17.10	15.45	2.69	9.6	0.42	34.0	139	66.0	269
3H-5, 30-35	17.60	15.95	2.74	9.6	0.41	15.1	59	84.9	335
3H-5, 55-60	17.85	16.20	2.77	9.6	0.40	15.7	61	84.3	327
3H-5, 105-110	18.35	16.70	2.82	9.6	0.41	23.8	93	76.2	299
3H-5, 130-135	18.60	16.95	2.85	9.6	0.41	39.5	157	60.5	240
3H-6, 30-35	19.10	17.45	2.90	9.6	0.42	32.0	130	68.0	276
3H-6, 55-60	19.35	17.70	2.92	9.6	0.43	25.3	104	74.7	307
3H-6, 105-110	19.85	18.20	2.98	9.6	0.43	26.8	110	73.2	302
3H-6, 130-135	20.10	18.45	3.00	9.6	0.43	25.8	106	74.2	305
4H-1, 30-35	21.10	20.40	3.20	9.6	0.42	17.2	70	82.8	336
4H-1, 55-60	21.35	20.65	3.23	9.6	0.42	19.9	81	80.1	324
4H-1, 105-110	21.85	21.15	3.28	9.6	0.42	18.3	74	81.7	328
4H-1, 130-135	22.10	21.40	3.31	9.6	0.42	11.7	47	88.3	353
4H-2, 30-35	22.60	21.90	3.36	9.6	0.41	23.1	92	76.9	305
4H-2, 55-60	22.85	22.62	3.44	9.6	0.41	19.4	77	80.6	319
4H-2, 105-110	23.35	23.27	3.50	9.6	0.39	11.9	44	88.1	329
4H-2, 130-135	23.60	23.60	3.54	9.6	0.37	14.0	50	86.0	309
4H-3, 30-35	24.10	24.25	3.64	6.0	0.34	7.5	15	92.5	191
4H-3, 55-60	24.35	24.58	3.69	6.0	0.33	7.4	15	92.6	183
4H-3, 105-110	24.85	25.24	3.80	6.0	0.32	6.3	12	93.7	182
4H-3, 130-135	25.10	25.55	3.85	6.0	0.32	8.3	16	91.7	179
4H-4, 30-35	25.60	26.05	3.93	6.0	0.33	8.5	17	91.5	180
4H-4, 55-60	25.85	26.30	3.98	6.0	0.33	7.0	14	93.0	184
4H-4, 105-110	26.35	26.80	4.06	6.0	0.33	6.4	13	93.6	183
4H-4, 130-135	26.60	27.05	4.10	6.0	0.32	5.6	11	94.4	183
4H-5, 30-35	27.10	27.55	4.18	6.0	0.32	4.1	8	95.9	182
4H-5, 55-60	27.35	27.80	4.23	6.0	0.31	4.4	8	95.6	179
4H-5, 105-110	27.85	28.30	4.31	6.0	0.31	2.9	5	97.1	183
4H-5, 130-135	28.10	28.55	4.35	6.0	0.31	3.7	7	96.3	182
4H-6, 30-35	28.60	29.05	4.43	6.0	0.32	5.2	10	94.8	181
4H-6, 55-60	28.85	29.30	4.47	6.0	0.32	5.0	10	95.0	182
4H-6, 105-110	29.35	29.80	4.56	6.0	0.31	3.7	7	96.3	178
5H-1, 30-35	30.60	30.30	4.64	6.0	0.26	3.9	6	96.1	152
5H-1, 54-59	30.84	30.54	4.68	6.0	0.26	2.5	4	97.5	150
5H-1, 105-110	31.35	31.05	4.77	6.0	0.26	4.9	8	95.1	151
5H-1, 130-135	31.60	31.30	4.81	6.0	0.27	6.8	11	93.2	154
5H-2, 30-35	32.10	31.80	4.89	6.0	0.29	5.4	10	94.6	168
5H-2, 54-59	32.34	32.04	4.93	6.0	0.30	12.9	24	87.1	159
5H-2, 105-110	32.85	32.55	5.01	6.0	0.34	6.1	12	93.9	192
5H-2, 130-135	33.10	32.80	5.06	6.0	0.36	14.0	30	86.0	186
5H-3, 30-35	33.60	33.30	5.14	6.0	0.40	14.9	36	85.1	204
5H-3, 54-59	33.84	33.54	5.18	6.0	0.42	12.8	32	87.2	220
5H-3, 105-110	34.35	34.05	5.26	6.0	0.43	10.6	28	89.4	234
5H-3, 130-135	34.60	34.30	5.31	6.0	0.44	11.3	30	88.7	234
5H-4, 30-35	35.10	34.80	5.39	6.0	0.44	9.6	26	90.4	242

Table 1 (continued).

Core, section interval (cm)	Depth (mbsf)	Depth (mcd)	Age (m.y.)	LSR (m/m.y.)	DBD (g/cm <sup>3</sup> )	Eolian (wt%)	Eolian MAR (mg/cm <sup>2</sup> ·k.y.)	Opal (wt%)	Opal MAR (mg/cm <sup>2</sup> ·k.y.)
5H-4, 54-59	35.34	35.04	5.43	6.0	0.45	19.5	53	80.5	217
5H-4, 105-110	35.85	35.55	5.51	6.0	0.43	13.2	34	86.8	225
5H-4, 130-135	36.10	35.80	5.55	6.0	0.42	12.7	32	87.3	219
5H-5, 30-35	36.60	36.30	5.64	6.0	0.39	10.5	25	89.5	211
5H-5, 54-59	36.84	36.54	5.68	6.0	0.38	10.0	23	90.0	205
5H-5, 105-110	37.35	37.05	5.76	6.0	0.37	9.7	22	90.3	201
5H-5, 130-135	37.40	37.10	5.77	6.0	0.37	10.3	23	89.7	200
5H-6, 30-35	38.10	37.80	5.89	6.0	0.37	10.9	24	89.1	198
5H-6, 54-59	38.34	38.04	5.93	6.0	0.37	12.6	28	87.4	195
5H-6, 105-110	38.85	38.55	6.01	6.0	0.40	16.4	39	83.6	200
5H-6, 130-135	39.10	38.80	6.05	6.0	0.41	10.0	25	90.0	225
5H-7, 30-35	39.60	39.30	6.14	6.0	0.45	18.6	50	81.4	221
5H-7, 54-59	39.84	39.54	6.18	6.0	0.47	24.9	70	75.1	212
6H-1, 30-35	40.10	39.80	6.22	6.0	0.46	17.2	48	82.8	229
6H-1, 54-59	40.34	40.04	6.26	6.0	0.42	16.8	42	83.2	209
6H-1, 130-135	41.10	41.25	6.46	6.0	0.41	9.1	22	90.9	222
6H-2, 30-35	41.60	41.75	6.54	6.0	0.42	15.6	39	84.4	213
6H-2, 54-59	41.84	41.99	6.58	6.0	0.43	15.3	39	84.7	217
6H-2, 105-110	42.35	42.50	6.67	6.0	0.42	15.3	39	84.7	214
6H-2, 130-135	42.60	42.75	6.71	6.0	0.41	12.5	31	87.5	218
6H-3, 30-35	43.10	43.25	6.79	6.0	0.40	12.9	31	87.1	210
6H-3, 54-59	43.34	43.49	6.83	6.0	0.39	9.3	22	90.7	215
6H-3, 105-110	43.85	44.00	6.92	6.0	0.38	3.8	9	96.2	219
6H-3, 130-135	44.10	44.25	6.96	6.0	0.37	6.1	14	93.9	209
6H-4, 30-35	44.60	44.75	7.04	6.0	0.35	8.7	19	91.3	194
6H-4, 54-59	44.84	44.99	7.08	6.0	0.35	9.6	20	90.4	188
6H-4, 105-110	45.35	45.50	7.17	6.0	0.37	12.1	27	87.9	194
6H-4, 130-135	45.60	45.75	7.21	6.0	0.38	12.9	30	87.1	202
6H-5, 30-35	46.10	46.25	7.28	8.1	0.42	8.6	29	91.4	314
6H-5, 54-59	46.34	46.49	7.31	8.1	0.44	14.3	51	85.7	307
6H-5, 105-110	46.85	47.00	7.37	8.1	0.45	17.8	66	82.2	305
6H-5, 130-135	47.10	47.25	7.40	8.1	0.46	24.0	89	76.0	284
6H-6, 30-35	47.70	47.85	7.47	8.1	0.47	34.7	132	65.3	248
6H-6, 54-59	47.84	47.99	7.49	8.1	0.47	32.6	124	67.4	257
6H-6, 105-110	48.35	48.50	7.55	8.1	0.46	32.4	123	67.6	256
6H-6, 130-135	48.60	48.75	7.59	8.1	0.46	28.6	107	71.4	268
6H-7, 30-35	49.10	49.25	7.65	8.1	0.45	29.1	107	70.9	262
6H-7, 55-60	49.35	49.50	7.68	8.1	0.45	25.1	92	74.9	274
7H-1, 30-35	49.60	50.85	7.84	8.1	0.45	23.7	86	76.3	277
7H-1, 55-60	49.85	51.19	7.89	8.1	0.44	21.1	76	78.9	284
7H-1, 105-110	50.35	51.88	8.42	1.2	0.45	34.5	19	65.5	36
7H-1, 130-135	50.60	52.22	8.70	1.2	0.45	44.4	24	55.6	30
7H-2, 30-35	51.10	52.85	9.22	1.2	0.46	43.1	24	56.9	32
7H-2, 55-60	51.35	53.10	9.43	1.2	0.47	42.7	24	57.3	32
7H-2, 105-110	51.85	53.60	9.84	1.2	0.52	44.4	28	55.6	35
7H-2, 130-135	52.10	53.85	10.05	1.2	0.56	40.9	28		
7H-3, 30-35	52.60	54.35	10.46	1.2	0.63	46.4	35		
7H-3, 55-60	52.85	54.60	10.66	1.2	0.66	42.4	34		
7H-3, 105-110	53.35	55.10	11.08	1.2	0.65	42.5	34		
7H-3, 130-135	53.60	55.35	11.28	1.2	0.64	32.7	25		
7H-4, 30-35	54.10	55.50	11.40	1.2	0.60	36.1	26		
7H-4, 55-60	54.35	55.57	11.47	1.2	0.58	32.5	23		
7H-4, 105-110	54.85	55.90	22.00	0.4	0.57	31.7	7		
7H-4, 130-135	55.10	56.09	22.51	0.4	0.58	29.4	6		
7H-5, 30-35	55.60	56.64	23.99	0.4	0.58	35.1	8		
7H-5, 55-60	55.85	56.96	24.83	0.4	0.59	35.3	8		
7H-5, 105-110	56.35	57.59	26.52	0.4	0.57	37.6	8		
7H-5, 130-135	56.60	58.06	27.78	0.4	0.55	31.5	6		
7H-6, 30-35	57.10	58.65	29.35	0.4	0.52	30.8	6		
7H-6, 55-60	57.35	58.86	29.92	0.4	0.51	26.4	5		
7H-6, 105-110	57.85	59.28	31.03	0.4	0.52	36.7	7		
7H-6, 135-140	58.15	59.43	31.43	0.4	0.54	32.1	7		
7H-7, 30-35	58.60	59.65	32.03	0.4	0.57	37.2	8		
7H-7, 55-60	58.85	59.78	32.37	0.4	0.55	35.5	7		
145-886C-									
7H-1, 30-35	54.60	53.56	9.80	1.2	0.36	43.1	19		
7H-1, 103-108	55.33	53.94	10.12	1.2	0.38	40.5	19		
7H-1, 130-135	55.60	54.08	10.23	1.2	0.44	38.4	20		
7H-2, 30-35	56.10	54.34	10.45	1.2	0.58	43.2	30		
7H-2, 55-60	56.35	54.47	10.55	1.2	0.65	41.2	32		
7H-2, 130-135	57.10	54.87	10.89	1.2	0.69	42.1	35		
7H-3, 30-35	57.60	55.15	11.12	1.2	0.69	40.2	34		
7H-3, 55-60	57.85	55.29	11.24	1.2	0.69	38.0	32		
7H-3, 105-110	58.35	55.75	11.61	1.2	0.66	36.8	30		
7H-3, 130-135	58.60	56.00	22.27	0.4	0.64	31.6	8		
7H-4, 30-35	59.10	56.50	23.61	0.4	0.60	31.7	7		
7H-4, 55-60	59.35	56.75	24.28	0.4	0.58	32.5	7		
7H-4, 105-110	59.85	57.25	25.62	0.4	0.56	34.7	7		
7H-4, 130-135	60.10	57.50	26.28	0.4	0.56	33.4	7		
7H-5, 30-35	60.60	58.00	27.62	0.4	0.55	32.5	7		
7H-5, 55-60	60.85	58.25	28.29	0.4	0.54	33.1	7		
7H-5, 105-110	61.35	58.75	29.63	0.4	0.51	28.5	5		
7H-5, 126-131	61.56	58.96	30.19	0.4	0.49	30.2	5		
7H-6, 30-35	62.10	59.50	31.63	0.4	0.51	33.4	6		
7H-6, 55-60	62.35	59.75	32.30	0.4	0.52	35.3	7		
7H-6, 105-110	62.85	60.25	33.64	0.4	0.57	34.9	7		
7H-6, 130-135	63.10	60.50	38.68	0.1	0.60	36.7	2		
7H-7, 30-35	63.60	61.00	45.47	0.1	0.64	39.2	2		

Table 1 (continued).

Core, section interval (cm)	Depth (mbsf)	Depth (mcd)	Age (m.y.)	LSR (m/m.y.)	DBD (g/cm <sup>3</sup> )	Eolian (wt%)	Eolian MAR (mg/cm <sup>2</sup> ·k.y.)	Opal (wt%)	Opal MAR (mg/cm <sup>2</sup> ·k.y.)
8H-1, 30-35	64.10	62.25	63.87	0.5	0.59	26.8	8		
8H-1, 55-60	64.35	62.50	64.33	0.5	0.56	25.5	7		
8H-1, 105-110	64.85	63.00	65.26	0.5	0.53	26.5	7		
8H-1, 130-135	65.10	63.25	65.72	0.5	0.53	25.2	7		
8H-2, 30-35	65.60	63.75	66.65	0.5	0.52	28.7	8		
8H-2, 55-60	65.85	64.00	67.11	0.5	0.51	26.3	7		
8H-2, 105-110	66.35	64.50	68.04	0.5	0.51	19.4	5		
8H-2, 130-135	66.60	64.75	68.50	0.5	0.51	21.1	6		
8H-3, 30-35	67.10	65.25	69.43	0.5	0.52	16.5	4		
8H-3, 55-60	67.35	65.50	69.89	0.5	0.52	13.8	4		
8H-3, 105-110	67.85	66.00	70.82	0.5	0.51	9.2	2		
8H-3, 130-135	68.10	66.25	71.29	0.5	0.50	7.3	2		
8H-4, 30-35	68.60	66.75	72.21	0.5	0.49	7.2	2		
8H-4, 55-60	68.85	67.00	72.68	0.5	0.48	6.8	2		
8H-4, 105-110	69.35	67.50	73.60	0.5	0.48	7.7	2		
8H-4, 130-135	69.60	67.75	74.07	0.5	0.48	7.8	2		
8H-5, 30-35	70.10	68.25	74.99	0.5	0.47	7.7	2		
8H-5, 55-60	70.35	68.50	75.46	0.5	0.47	9.7	2		
8H-5, 105-110	70.85	69.00	76.38	0.5	0.46	8.8	2		
8H-6, 30-35	71.60	69.75	77.77	0.5	0.45	3.0	1		

Note: DBD = dry bulk density, LSR = linear sedimentation rate, and MAR = mass accumulation rate.

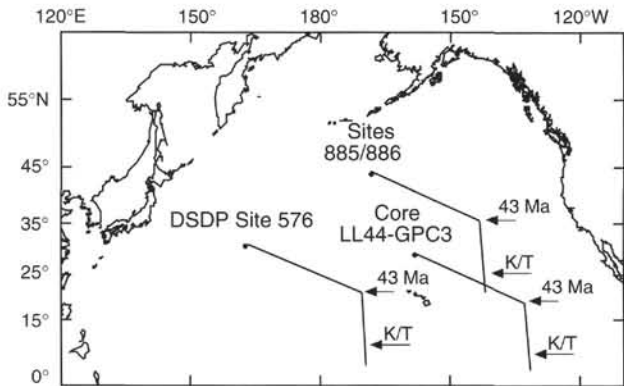


Figure 3. Present location of ODP Sites 885/886, DSDP Site 576, and piston Core LL44-GPC3. Lines are pale-backtrack paths. Plate rotation model is from van Andel et al. (1975). K/T = Cretaceous/Tertiary boundary.

and increases to approximately 80% toward the bottom of Unit I (Fig. 6). Opaline silica is the dominant component in Unit II, occupying at least 80% of the sediment for most of the unit (Fig. 6). Below 46 mcd, opal becomes less important in the total sediment makeup (Fig. 6). No microfossils suitable for biostratigraphy were found below 53 mcd (Rea, Basov, Janecsek, Palmer-Julson, et al., 1993). Onboard measurements of DBD and porosity indicate an increase in DBD of 0.16–0.31 g/cm<sup>3</sup> and a decrease in porosity of 6–11% between Samples 145-885A-6H-3, 74 cm and -6H-4, 74 cm, between 145-886B-7H-2, 69 cm and -7H-3, 69 cm, and between 886C-7H-1, 109 cm and -7H-2, 69 cm (Rea, Basov, Janecsek, Palmer-Julson, et al., 1993). Opaline silica-bearing sediments are usually characterized by lower DBD and higher porosity than opal-free sediments. Based on those two parameters, the transition from fossil-bearing to barren sediments is bracketed between 54 mcd and 54.5 mcd. A visual examination of smear-slides from samples in this interval shows the presence of some biogenic opal debris in samples shallower than 54.1 mcd but none in samples below 54.3 mcd.

### Mass Accumulation Rates: the Time Frame

The age model, based on the stratigraphic data (Table 2), is depicted as an age-depth plot in Figure 2A. The plot shows steep slopes in Units I and II, indicating fast sedimentation rates (Fig. 2B). Unit I extends back to approximately 3.55 Ma, whereas Unit II extends back to about 11 Ma. The LSRs between 0 and 2.6 Ma average 5 m/m.y.,

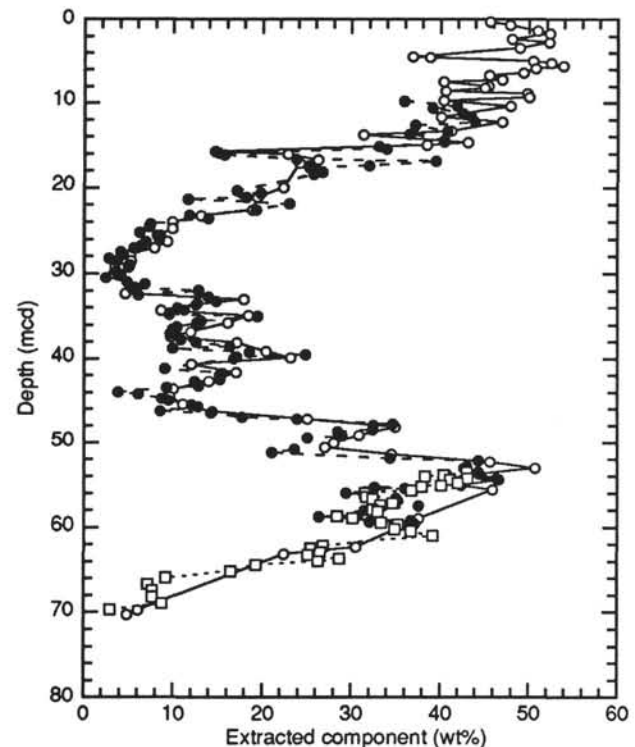


Figure 4. Abundance (in weight percent) of the extracted eolian component of sediments at Sites 885/886. The record for Hole 885A is represented by open circles connected by a solid line, the record for Hole 886B is represented by solid circles connected by a long-dashed line, and the record for Hole 886C is represented by open squares connected by a short-dashed line. All samples were placed on a composite depth scale. Note excellent correspondence of records from different holes.

and increase to approximately 6.5 m/m.y. from 2.6 to 7.25 Ma (Fig. 2B). There is a distinct decrease in LSR toward the bottom of Unit II, equivalent to the time interval between 8.5 and 11 Ma (Fig. 2B). A break in the age-depth relationship at 55 mcd marks the boundary between Units II and III and may indicate a hiatus occurring between approximately 11 and 20 Ma based on <sup>87</sup>Sr/<sup>86</sup>Sr stratigraphy (Fig. 2A). A hiatus at this depth was suggested by Dickens et al. (this volume). Ichthyoliths allowed us to determine the age-depth relationship for

Table 2. Stratigraphic control data, Sites 885/886.

Paleomagnetostratigraphy					
Magnetic reversal	Core, section, interval (cm)	Depth (mbsf)	Depth (mcd)	Age (m.y.)	Source
Brunhes/Matuyama			4.88	0.780	1
Termination Jaramillo			5.71	0.984	1
Onset Jaramillo			6.20	1.049	1
Termination Olduvai			9.55	1.757	1
Onset Olduvai			10.52	1.983	1
Matuyama/Gauss			14.58	2.600	1
Gauss/Gilbert			23.75	3.553	1
Termination C4n.1n			45.98	7.245	1
Onset C4n.2n			51.25	7.892	1
Termination C4An			52.01	8.529	1
Biostratigraphy					
Radiolarian event					
LO <i>S. acquilonium</i>	145-885A-1H-1, 115 and -1H-2, 115	1.15–2.65	1.54–3.67	0.4	2
LO <i>S. umiversus</i>	145-885A-1H-1, 115 and -1H-2, 115	1.15–2.65	1.54–3.67	0.55	2
LO <i>L. heteroporos</i>	145-885A-1H-1, 115 and -1H-2, 115	1.15–2.65	6.56–8.10	1.7	2
FO <i>C. davisiana davisiana</i>	145-885A-2H-5, 115 and -2H-6, 115	11.75–13.25	14.86–16.91	2.9	2
FO <i>L. heteroporos</i>	145-885A-5H-2, 115 and -5H-3, 115	35.75–37.25	41.83–43.78	6.5	2
T <i>S. delmontensis-S. peregrina</i>	145-885A-5H-5, 115 and -5H-6, 115	40.25–41.75	47.35–49.34	7.55	2
FO <i>S. acquilonium</i>	145-885A-5H-6, 115 and -6H-1, 115	41.75–43.75	49.34–51.57	7.72	2
LO <i>L. nipponica magnacornuta</i>	145-885A-6H-1, 115 and -6H-2, 115	43.75–45.25	51.57–53.24	8.8	2
LO <i>S. acquilonium</i>	145-886C-1H-1, 114 and -1H-2, 114	1.14–2.64	1.14–2.64	0.4	2
LO <i>S. umiversus</i>	145-886C-1H-2, 114 and -1H-3, 114	2.64–4.14	2.64–4.14	0.55	2
LO <i>L. heteroporos</i>	145-886C-1H-4, 114 and -2H-1, 114	5.64–7.94	5.84–9.30	1.7	2
FO <i>C. davisiana davisiana</i>	145-886C-3H-1, 114 and -3H-2, 114	17.44–18.94	15.29–16.99	2.9	2
FO <i>L. heteroporos</i>	145-886C-5H-3, 98 and -6H-1, 114	39.28–45.94	37.9–44.63	6.5	2
T <i>S. delmontensis-S. peregrina</i>	145-886C-6H-3, 112 and -6H-4, 114	48.92–50.44	47.51–49.04	7.55	2
FO <i>S. acquilonium</i>	145-886C-6H-4, 114 and -6H-5, 114	50.44–51.94	49.04–50.54	7.72	2
LO <i>L. nipponica magnacornuta</i>	145-886C-6H-5, 114 and -6H-CC	51.94–54.3	50.54–52.90	8.5	2
Sr-isotope stratigraphy					
	145-885A-6H-1, 125–130	43.85	51.69	5.7	3
	145-885A-6H-2, 50–55	44.60	52.64	5.9	3
	145-885A-6H-4, 50–55	47.60	55.29	21.3	3
	145-885A-6H-4, 125–130	48.35	55.90	19.4	3
	145-885A-6H-5, 50–55	49.10	59.68	30.2	3
	145-885A-7H-CC*	52.10	70.70	79.0	3
	145-886B-7H-2, 47–52	51.27	53.02	6.5	3
	145-886B-7H-3, 135–140	53.67	55.37	11.3	3
	145-886B-7H-4, 47–52	54.27	55.55	11.1	3
	145-886B-7H-4, 125–130	55.05	56.05	24.0	3
	145-886B-7H-4, 135–140	55.17	56.14	21.5	3
	145-886B-7H-5, 120–125	56.52	57.87	27.8	3
	145-886B-7H-6, 140–145	58.22	59.46	30.7	3
	145-886B-7H-7, 47–52	58.77	59.74	31.3	3
	145-886B-7H-7, 64–69	58.94	59.82	31.2	3
	145-886C-6H-4, 135–140	50.30	48.90	5.8	3
	145-886C-6H-7, 60–65	54.40	53.00	6.1	3
	145-886C-7H-2, 135–140	57.15	54.90	11.0	3
	145-886C-7H-3, 11–16	57.41	55.04	11.0	4
	145-886C-7H-3, 135–140	58.65	56.05	21.0	3
	145-886C-7H-4, 135–140	60.17	57.57	28.5	3
	145-886C-7H-5, 120–125	61.52	58.92	34.0	3
	145-886C-7H-6, 10–15	61.90	59.30	32.8	4
	145-886C-8H-1, 135–140	65.15	63.30	65.0	3
	145-886C-8H-2, 10–15	65.40	63.55	33.6	4
	145-886C-8H-4, 30–35	68.60	66.75	68.5	4
	145-886C-8H-4, 45–50	68.75	66.90	71.5	4
	145-886C-8H-4, 135–140	69.60	67.75	72.5	3
	145-886C-8H-5, 120–125	71.00	69.15	76.5	3
	145-886C-8H-6, 75–80	72.05	70.20	74.5	4
Ir anomaly	145-886C-8H-1,130 and -8H-1,145	65.1–65.25	63.25–63.40	66	5
Ar/Ar dating	Basement	52.30	70.95	80	6

Notes: mcd = meters composite depth. LO = last occurrence, FO = first occurrence, T = species transition. 1 = Rea, Basov, et al. (1993); 2 = Morley and Nigrini (this volume); 3 = Ingram (this volume); 4 = this paper; 5 = Kyte and Zhou (this volume); 6 = Keller and Duncan (this volume). \* = this sample is listed as 145-885A-7H-CC. However, Core 7H has no core catcher. We assume this sample is 145-885A-6H-CC.

the time interval between approximately 20 and 34 Ma, equivalent to the depth interval between 56 to 60 mcd (Fig. 2A). The LSRs between ~34 and 63 Ma, represented by 1.5 m of sediments and a 0.75-m core gap (Dickens et al., this volume), are low, and occurrences of hiatuses are likely (Fig. 2A). However, the possibility of resolving this part of the sediment record using the seawater Sr- isotope curve is small because  $^{87}\text{Sr}/^{86}\text{Sr}$  ratios do not vary much in this time interval. The difference in slope in the age-depth plot between Units I and II compared with Subunit IIIA attests to biogenous sedimentation as the

driving force in the rate of sedimentation (Fig 2A). In Subunit IIIB, however, hydrothermal sedimentation may be the controlling factor. Sedimentation rates between the K/T boundary and the basement average 0.5 m/m.y. An exponential increase in LSR toward the basement is predicted by the hydrothermal activity model for the first 15 m.y. (Dickens and Owen, this volume). An exponential best fit curve through the  $^{87}\text{Sr}/^{86}\text{Sr}$  ages in Core 886C-8H yields ages that are 1.8–2.2 m.y. younger than those obtained by linear regression between the K/T boundary and the basement. There is no significant dif-

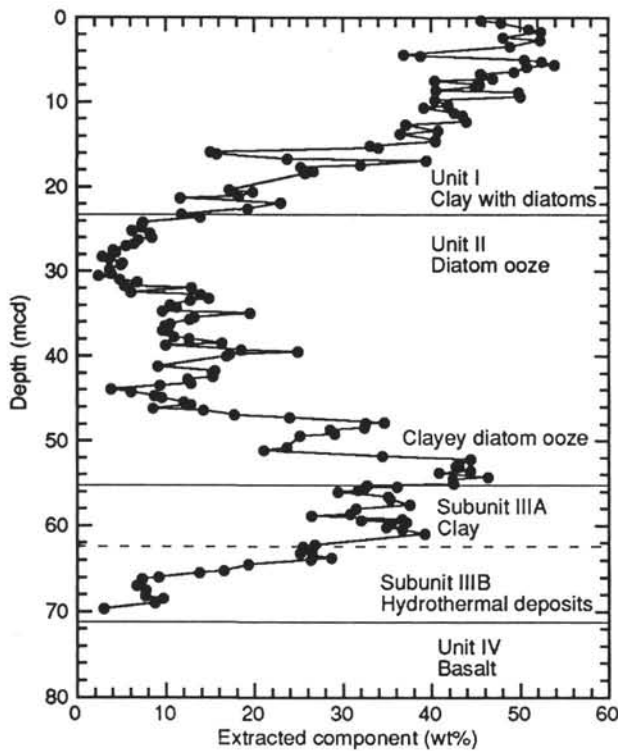


Figure 5. Record of eolian abundances at Sites 885/886 with lithostratigraphy on right-hand side. The eolian record has been assembled from data obtained in the top 10.25 mcd in Hole 885A, between 10.25 and 60 mcd in Hole 886B, and between 60 mcd and basement (at 70.95 mcd) in Hole 886C. Lithologic units are from Rea, Basov, Janecek, Palmer-Julson, et al. (1993), as modified by Dickens et al. (this volume).

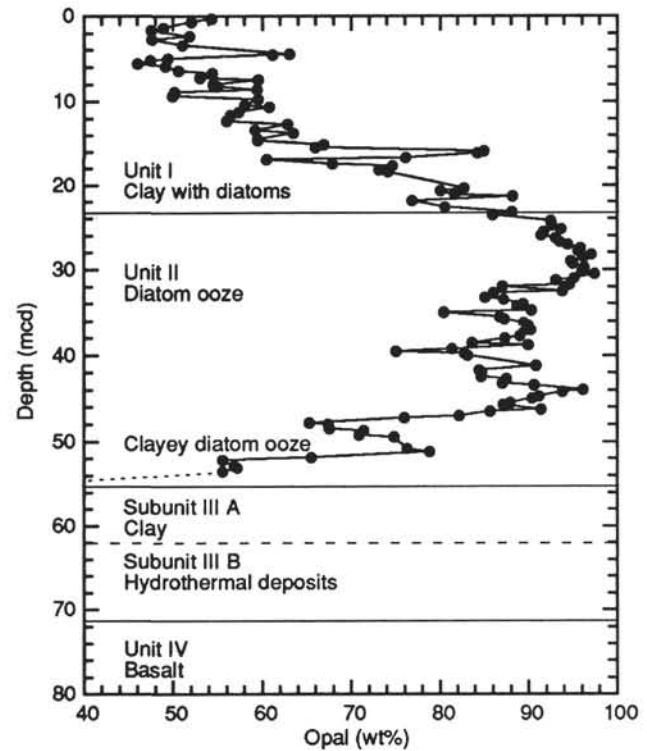


Figure 6. Record of opal abundances at Sites 885/886. The opal record has been assembled from data obtained in the top 10.25 mcd of Hole 885A, and between 10.25 and 55 mcd of Hole 886B. The sediment column is barren of siliceous microfossils below ~54 mcd, (i.e., in Subunits IIIA and IIB). Lithologic units are from Rea, Basov, Janecek, Palmer-Julson, et al. (1993), as modified by Dickens et al. (this volume).

ference in the eolian MAR. In view of the uncertainties of the  $^{87}\text{Sr}/^{86}\text{Sr}$  stratigraphy determined on ichthyoliths (see above) and the sampling resolution of the fish teeth, we prefer the linear interpolation approach.

Several unexpected values in the LSRs are emphasized in Figure 2. Suspect high LSRs occur between 0.984 and 1.049 Ma, between 2.6 and 3.553 Ma, and between 7.245 and 7.892 Ma. These values are a consequence of closely spaced "age-picks." Although not necessarily wrong, these high LSRs lead to anomalously high MARs compared to MARs calculated from LSRs averaged over more widely spaced "age-picks."

### Eolian Mass Accumulation Rates

Eolian fluxes were low, that is less than  $10 \text{ mg}/(\text{cm}^2 \text{ 148 k.y.})$  for most of the history of the sites (Fig. 7). A slight increase in eolian MARs at the end of the Cretaceous is probably the result of LSR averaging and not indicative of paleoclimate in the Late Cretaceous and Paleocene. Eocene sediments occur in negligible amounts. During the Oligocene and earliest Miocene, eolian sediments were deposited, but fluxes remained low ( $10 \text{ mg}/(\text{cm}^2 \text{ 148 k.y.})$ ) (Fig. 7). The first eolian deposition of note occurs at approximately 11 Ma (Figs. 7 and 8). Eolian accumulation for most of the late Miocene fluctuates around  $30 \text{ mg}/(\text{cm}^2 \text{ 148 k.y.})$ . An exception in this trend is the sudden spike in eolian MARs between 7.8 and 7.2 Ma (Fig. 8), a consequence in part of the presence of a large eolian component but probably caused more so by elevated LSRs. Eolian fluxes are very low (less than  $10 \text{ mg}/(\text{cm}^2 \text{ 148 k.y.})$ ) in the early Pliocene, at the high tide of the "Diatom Dump" (Fig. 8). At ~3.5 Ma, fluxes increased rapidly to reach maxima in excess of  $120 \text{ mg}/(\text{cm}^2 \text{ 148 k.y.})$  between 2.6 and 2.0 Ma. Fluxes in the younger sediments vary from ~90 to  $100 \text{ mg}/(\text{cm}^2 \text{ 148 k.y.})$  in the early Pleistocene and from ~130–150  $\text{mg}/(\text{cm}^2 \text{ 148 k.y.})$  for the last 1 m.y.

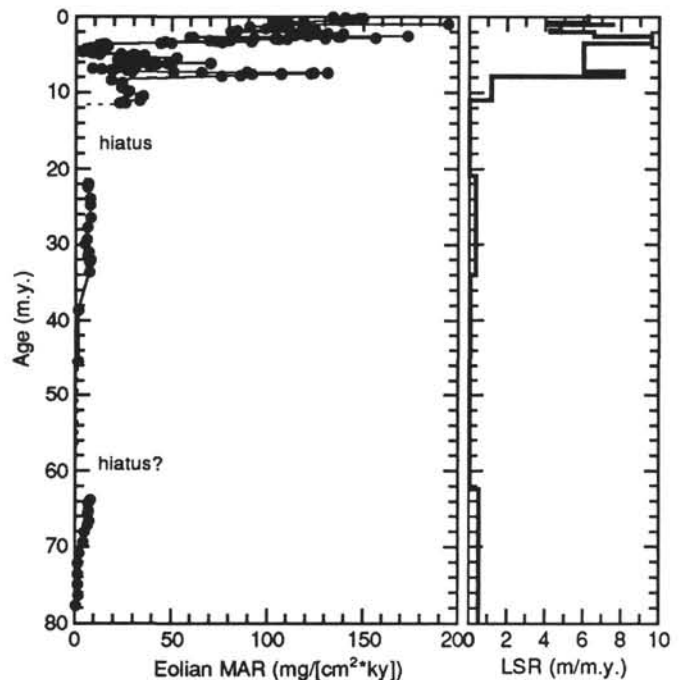


Figure 7. Mass accumulation rates (MAR) of eolian sediment at Sites 885/886 during the past 80 m.y. Linear sedimentation rates (LSR) shown for reference.

Table 3. Fish teeth Sr-isotopic results.

Core, section, interval (cm)	Depth (mbsf)	Depth (mcd)	Notes	Visible oxides	$^{87}\text{Sr}/^{86}\text{Sr} \pm 2\sigma$
145-886C-					
6H-4, 100-105	50.30	48.90	2 teeth	No	0.708949 $\pm$ 45
6H-7, 60-65	54.40	53.00	8 teeth	No	0.708926 $\pm$ 24
7H-3, 11-16	57.41	55.04	7 teeth	No	0.708846 $\pm$ 13
7H-6, 10-15	61.90	59.30	7 teeth	No	0.707965 $\pm$ 17
8H-2, 10-15	65.40	63.55	8 tiny teeth	Yes	0.707939 $\pm$ 17
8H-4, 30-35	68.60	66.75	1 big tooth	Yes	0.707749 $\pm$ 15
8H-4, 45-50	68.75	66.90	4 teeth	Yes	0.707698 $\pm$ 15
8H-6a, 75-80	72.05	70.20	1 big bored tooth	Yes	0.707617 $\pm$ 20
8H-6b, 75-80	72.05	70.20	9 tiny teeth	Yes	0.707809 $\pm$ 17
NBS 987					
(analyzed twice)					0.710246 $\pm$ 17
Long-term					
NBS 987 average					0.710248 $\pm$ 18

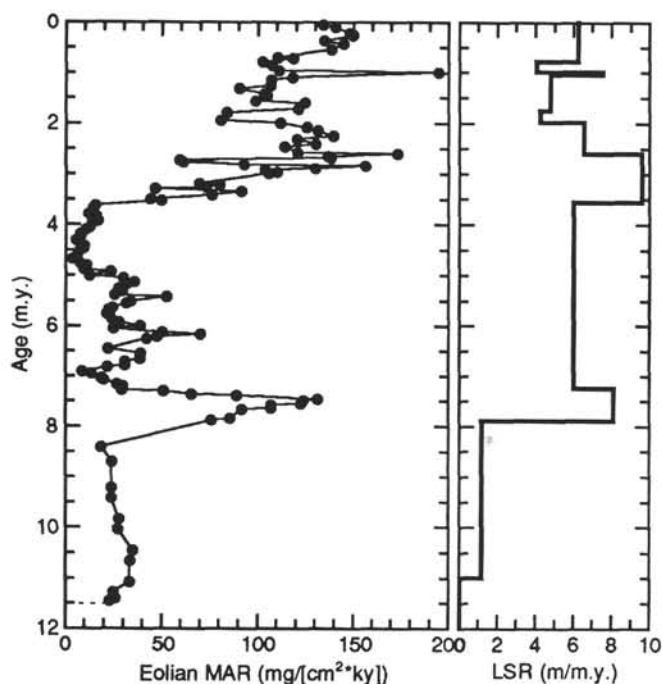


Figure 8. MAR of eolian sediment at Sites 885/886 during the past 11 m.y. Eolian fluxes increased markedly in the late Pliocene, corresponding to the onset of Northern Hemisphere glaciation. Increased fluxes between 2.6 and 3.5 Ma and between 7.2 and 7.8 Ma are probably artifacts of the linear sedimentation rate. LSR shown for reference.

### Opal Mass Accumulation Rates

The oldest sediments with an identifiable siliceous microfossil assemblage are approximately 9 m.y. old (Joe Morley, pers. comm., 1994). Based on changes in DBD and porosity of the sediment, the visual examination of smear slides (see above), and our age model, which is partly based on ichthyolith-ages, we determine the age of the oldest opal-bearing sediment between 10 and 10.5 Ma (Fig. 9). Opal deposition remained low during the first 2 m.y. but it was well underway at 8 Ma. The abrupt rise in opal MAR at 8 Ma may be an artifact of the exceptional LSRs mentioned above (Fig. 9). The details in the opal record are LSR driven. The failure to distinguish the interval of increased silica deposition clearly between approximately 6 and 3 Ma, as seen in all other Leg 145 sites, (especially the somewhat puzzling low accumulation between 5 and 3.5 Ma) may be caused by the choice of the "master section" for the composite depth for this interval. Dickens et al. (this volume) suggest that the composite depth

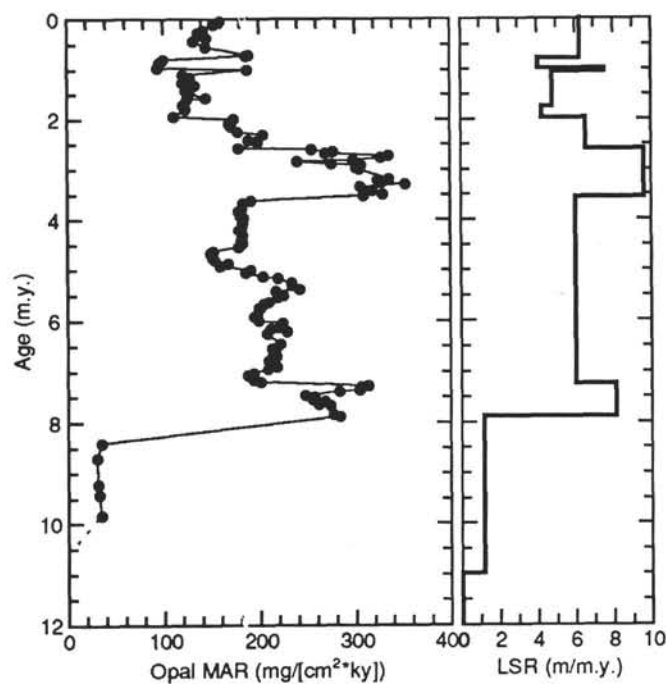


Figure 9. MAR of opal at Sites 885/886 during the past 11 m.y. Opal fluxes during the Pliocene "silica dump" are 1.5 to 2 times higher than fluxes during the Pleistocene. The height of the flux between 2.6 and 3.5 Ma and the rapid increase in opal flux at 7.8 Ma are artifacts of the LSR, shown for reference.

at about 30 mcd may be ~1.5 m too short because of compression caused by drilling through soft diatom ooze. However, the overall picture clearly shows 1.5–2 times higher opal fluxes during the late Miocene and early Pliocene than in the period after 2.6–2 Ma. There may be a stepwise(?) increase in opal MAR at about 1 Ma from 120 to 160 mg/(cm<sup>2</sup> 148 k.y.) in the late Pleistocene.

### DISCUSSION

The record of eolian fluxes at Sites 885/886 at a location that is 12°–14°N of DSDP Site 576 and piston Core LL44-GPC3 (Fig. 3) provides an excellent addition to the knowledge of paleoclimate gathered from those well-studied records.

As in Sites 885/886, much of the time scale for Core LL44-GPC3 has been derived based on different, uncommon tools, whose use have lead to different interpretations. In presenting the depositional history for this red clay core we have used the time scale published by Janecek and Rea (1983). The stratigraphy is based largely on fish teeth (Doyle and Riedel, 1979) along with magnetic reversal stratigraphy down to the Matuyama/Gauss boundary (Prince et al., 1980). Leinen and her co-workers (including Rea et al., 1985; Doh et al., 1988; and Leinen, 1989) show a somewhat different stratigraphy, also based on ichthyoliths. This version has accumulation peaks in the lower and middle Miocene part of the section. Kyte et al. (1993) have generated a third age-model for this core based on the assumption that cobalt accumulates at a constant rate in the sediments throughout the Tertiary, and on the discovery of the Ir anomaly associated with the Cretaceous/Tertiary boundary at a depth of 20.6 mbsf (Kyte and Wasson, 1986). The presence of three age models in the literature for the same core points out the need for a reliable stratigraphic tool with which to date the pelagic clays of the abyssal oceans.

All three sites have records which extend back into the Late Cretaceous. During the Late Cretaceous and the Paleocene eolian MARs at DSDP Site 576 and in Core LL44-GPC3 were low (Fig. 10), corresponding to warm and wet climates (Janecek, 1985). Furthermore,

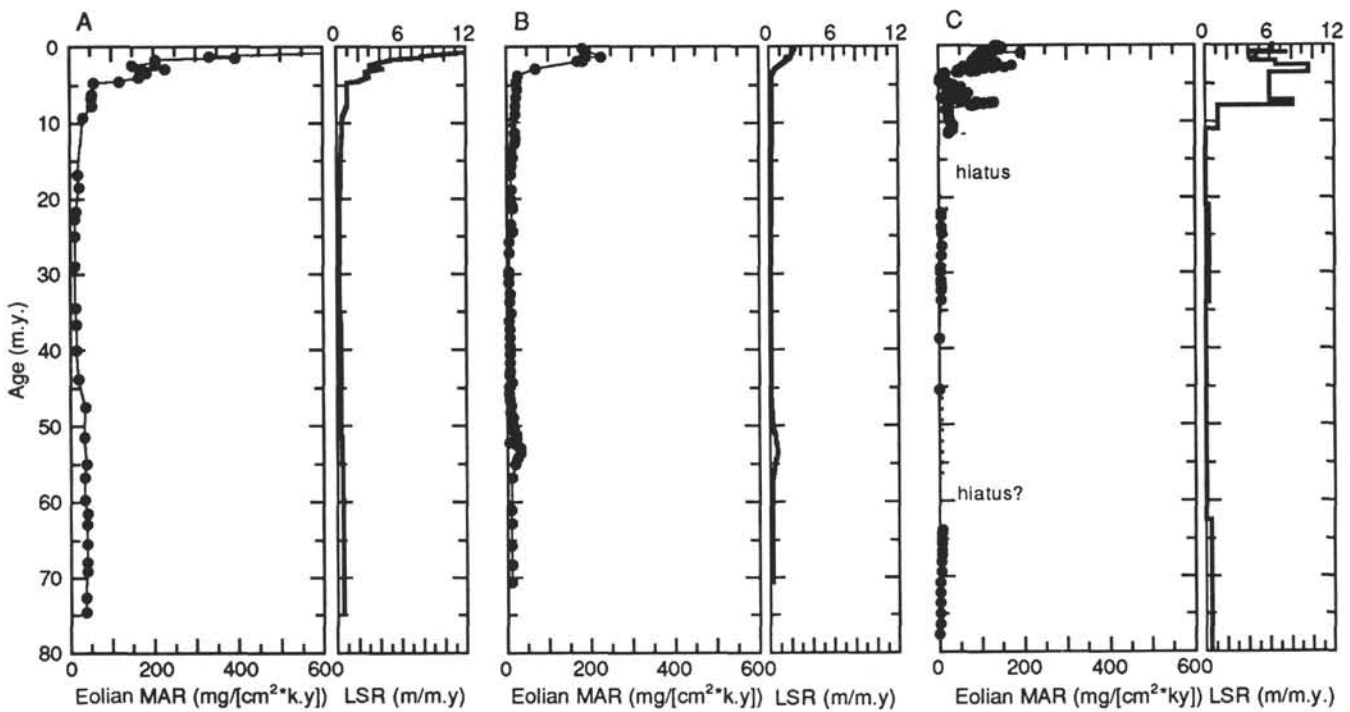


Figure 10. A. MAR of eolian sediment at DSDP Site 576 (32°N, 164°E) during the past 75 m.y. (Janecek, 1985); B. MAR in piston Core LL44-GPC3 (30°N, 158°W) during the past 70 m.y. (Janecek and Rea, 1983); C. MAR at Sites 885/886. LSR shown for reference.

during the middle and late Eocene, the records show a further decrease in eolian MARs (Fig. 10). This decrease was interpreted as the result of a more humid climate in the eolian source region and/or the passage of those sites from one wind belt to another (Leinen and Heath, 1981; Janecek and Rea, 1983; Rea, 1994). Our results show no exception: accumulation during the Cretaceous is low, and (nearly) nonexistent during the later part of the Paleocene and during the Eocene. Because ODP Sites 885/886 are situated north of the other sites, and because the Pacific Plate moved northward (Fig. 3), the movement of Sites 885/886 from one wind belt to another should have occurred earlier. The record at Sites 885/886 does not provide evidence for this event. Low accumulation rates at DSDP Site 576 (Janecek, 1985) during the Oligocene contrast with our results. Higher eolian fluxes during the time interval between ~20 and 34 Ma suggest drier conditions in the source area. The onset of this interval may be coincident with the appearance of ice-rafted debris in the Southern Ocean at about 34 Ma and glaciological evidence for ice cover on Antarctica (Crowley and North, 1991). The age resolution provided by the fish teeth does not allow precise determination of the onset of this interval. The beginning of the Neogene is characterized by a doubling of the eolian accumulation (from very low to low) in Core LL44-GPC3 (Janecek and Rea, 1985) and at DSDP Site 576. This increase is thought to reflect the initiation of deposition from the westerlies at those sites as they moved under its influence (Janecek and Rea, 1985). If a similar increase in flux is present at Sites 885/886, it remains unresolved within the resolution of the Sr-isotope stratigraphy.

Eolian accumulation increases at 11 Ma, shortly before sediments begin to contain microfossils. Accumulation of the biogenic silica increases rapidly after 8 Ma, which would be over 1 m.y. earlier than at the other Leg 145 sites, in which the kick off to the "Diatom Dump" occurs at 6–7 Ma (Rea and Snoeckx, this volume). An earlier onset of increased silica deposition may reflect the sensitivity of a marginal area to changes in and expansion of the high-productivity zone of the North Pacific. It is clear that a silica shift did occur at Sites 885/886 and although fluxes are smaller than at the other Leg 145 sites, they

signify at least a fivefold increase compared with older sediments and 1.5–2 times the accumulation in younger sediments.

The flux of the windblown sediments increases from 3.5 Ma on to reach the highest eolian MARs during the late Pliocene and Pleistocene. A similar pattern was observed in Core LL44-GPC3 (Janecek and Rea, 1985) and at DSDP Site 576 (Janecek, 1985); it reflects the drying of the Asian source region before and after the onset of Northern Hemisphere glaciation at 2.6 Ma.

## CONCLUSIONS

The sediment column of Sites 885/886 records the history of eolian deposition for much of the Cenozoic and latest Late Cretaceous. The record contains hiatuses between 11 and 20 Ma and probably also in the Eocene and Paleocene.

Eolian fluxes were low in the Late Cretaceous and early Cenozoic as a consequence of the humid conditions thought to have prevailed at that time.

The flux of windblown sediments during the Oligocene reflects the drier climate conditions in the source area. The increased aridity is coincident with the expansion(?) of Antarctic glaciation and a general cooling and drying of the Northern Hemisphere.

The "Diatom Dump," an interval of increased opal accumulation in the late Miocene to middle Pliocene, extends areally to Sites 885/886. Although fluxes are smaller than at the other Leg 145 sites, they signify a two- to fivefold increase to fluxes before and after the event.

A fivefold increase in eolian MARs beginning at 3.5 Ma testifies to the arid conditions that dominated continental climate at the onset of Northern Hemisphere glaciation.

## ACKNOWLEDGMENTS

We thank everyone on Leg 145 for the company and the learning experience during the cruise. This manuscript was reviewed by William Balsam and John King whose useful suggestions greatly

improved this manuscript. We also like to acknowledge the help of Joe Morley with biostratigraphic data. We also thank Karen Boven, Angela Walker, and Pamela Warner for help in the lab. This research was supported by the U.S. Science Support Program of the Joint Oceanographic Institutions.

## REFERENCES\*

- Bertram, C.J., Elderfield, H., Aldridge, R.J., and Conway-Morris, S., 1992.  $^{87}\text{Sr}/^{86}\text{Sr}$ ,  $^{143}\text{Nd}/^{144}\text{Nd}$ , and REE's in Silurian phosphatic fossils. *Earth Planet. Sci. Lett.*, 113:239–249.
- Cande, S.C., and Kent, D.V., 1992. A new geomagnetic polarity time scale for the Late Cretaceous and Cenozoic. *J. Geophys. Res.*, 97:13917–13951.
- Crowley, T.J., and North, G.R., 1991. *Paleoclimatology: Oxford Monographs on Geology and Geophysics*. New York (Oxford Univ. Press).
- Doh, S.-J., King, J.W., and Leinen, M., 1988. A rock-magnetic study of giant piston core LL4-GPC3 from the central North Pacific and its paleoceanographic implications. *Paleoceanography*, 3:89–111.
- Dole, P.S., and Riedel, W.R., 1979. Cretaceous to Neogene ichthyoliths in a giant piston core from the central North Pacific. *Micropaleontology*, 25:337–364.
- Hovan, S.A., in press. Late Cenozoic atmospheric circulation intensity and climatic history recorded by eolian deposition in the eastern equatorial Pacific Ocean, Leg 138. In Pisias, N.G., Mayer, L.A., Janecek, T.R., Palmer-Julson, A., and van Andel, T.H. (Eds.), *Proc. ODP, Sci. Results*, 138: College Station, TX (Ocean Drilling Program).
- Janecek, T.R., 1985. Eolian sedimentation in the Northwest Pacific Ocean: a preliminary examination of the data from Deep Sea Drilling Project Sites 576 and 578. In Heath, G.R., Burckle, L.H., et al., *Init. Repts. DSDP*, 86: Washington (U.S. Govt. Printing Office), 589–603.
- Janecek, T.R., and Rea, D.K., 1983. Eolian deposition in the northeast Pacific Ocean: Cenozoic history of atmospheric circulation. *Geol. Soc. Am. Bull.*, 94:730–738.
- Kyte, F.T., Leinen, M., Heath, G.R., and Zhou, L., 1993. Cenozoic sedimentation history of the central North Pacific: inferences from the elemental geochemistry of Core LL44-GPC3. *Geochim. Cosmochim. Acta*, 57:1719–1740.
- Kyte, F.T., and Wasson, J.T., 1986. Accretion rate of extraterrestrial matter: iridium deposited 33 to 67 million years ago. *Science*, 232:1225–1229.
- Leinen, M., 1989. The pelagic clay province of the North Pacific Ocean. In Winterer, E.L., Hussong, D.M., and Decker, R.W. (Eds.), *The Geology of North America* (Vol. N): *The Eastern Pacific Ocean and Hawaii*. *Geol. Soc. Am.*, 323–335.
- Leinen, M., and Heath, G.R., 1981. Sedimentary indicators of atmospheric circulation in the Northern Hemisphere during the Cenozoic. *Palaeogeogr., Palaeoclimatol., Palaeoecol.*, 36:1–21.
- Mehra, O.P., and Jackson, M.L., 1960. Iron oxide removal from soils and clays by a dithionite-citrate system buffered with sodium bicarbonate. *Clays Clay Miner., Proc. Conf.*, 7:317–327.
- Nakai, S., Halliday, A.N., and Rea, D.K., 1993. Provenance of dust in the Pacific Ocean. *Earth Planet. Sci. Lett.*, 119:143–157.
- Prince, R.A., 1978. Southward motion of the Hawaiian hotspot between 42 and 25 MYBP. *Geol. Soc. Am. Abstr. Progr.*, 10:474.
- Prince, R.A., Heath G.R., and Kominz, K., 1980. Paleomagnetic studies of the central north Pacific sediment cores: stratigraphy, sedimentation rates, and the origin of magnetic instability. *Geol. Soc. Am. Bull. (Pt. 2)*, 91:1789–1835.
- Prospero, J.M., 1981. Eolian transport to the world ocean. In Emiliani, C. (Ed.), *The Sea* (Vol. 7): *The Oceanic Lithosphere*. New York (Wiley), 801–874.
- Pye, K., 1989. Processes of fine particle formation, dust source regions, and climatic changes. In Leinen, M., and Sarnthein, M. (Eds.), *Paleoclimatology and Paleometeorology: Modern and Past Patterns of Global Atmospheric Transport*. Boston (Kluwer Acad. Publ.), 3–30.
- Rea, D.K., 1994. The paleoclimatic record provided by eolian deposition in the deep sea—the geologic history of wind. *Rev. Geophys.*, 32:159–195.
- Rea, D.K., Basov, I.A., Janecek, T.R., Palmer-Julson, A., et al., 1993. *Proc. ODP, Init. Repts.*, 145: College Station, TX (Ocean Drilling Program).
- Rea, D.K., and Harrsch, E.C., 1981. Mass accumulation rates of the non-authigenic inorganic crystalline (eolian) component of deep sea sediments from Hess Rise, Deep Sea Drilling Program Sites 464, 465, and 466. In Thiede, J., Vallier, T.L., et al., *Init. Repts. DSDP*, 62: Washington (U.S. Govt. Printing Office), 661–668.
- Rea, D.K., and Janecek, T.R., 1981. Mass-accumulation rates of the non-authigenic inorganic crystalline (eolian) component of deep-sea sediments from the western mid-Pacific Mountains, Deep Sea Drilling Project Site 463. In Thiede, J., Vallier, T.L., et al., *Init. Repts. DSDP*, 62: Washington (U.S. Govt. Printing Office), 653–659.
- Rea, D.K., Leinen, M., and Janecek, T.R., 1985. A geological approach to the long-term history of atmospheric circulation. *Science*, 227:721–725.
- Staudigel, H., Dole, P., and Zindler, A., 1985. Sr and Nd isotope systematics in fish teeth. *Earth Planet. Sci. Lett.*, 76:45–56.
- van Andel, T.H., Heath, G.R., and Moore, T.C., Jr., 1975. Cenozoic history and paleoceanography of the central equatorial Pacific Ocean: a regional synthesis of Deep Sea Drilling Project data. *Mem.—Geol. Soc. Am.*, 143.

\* Abbreviations for names of organizations and publications in ODP reference lists follow the style given in *Chemical Abstracts Service Source Index* (published by American Chemical Society).

Date of initial receipt: 4 April 1994  
Date of acceptance: 19 September 1994  
Ms 145SR-123